Rheology and agglomeration behavior of semi-crystalline polyamide powders for selective laser sintering: A comparative study of PA11 and PA12 formulations

Mohamad Mahmoud, Brendan Huitorel, Abdoulaye Fall

Rheology and Agglomeration Behavior of Semi-Crystalline Polyamide Powders for Selective Laser Sintering: A Comparative Study of PA11 and PA12 Formulations

Mohamad Mahmoud[a], Brendan Huitorel[b], Abdoulaye Fall[a,*]

[a]*Laboratoire NAVIER, UMR 8205-Université Gustave Eiffel, Ecole des Ponts, CNRS, Bâtiment Bienvenue 14-20 Boulevard Newton Champs-sur-Marne, 77420, France*
[b]*Arkema-CERDATO, Route du Rilsan, 27470, Serquigny, France*

Abstract

In this study, we investigated the rheological behavior of various polyamide powders as a function of temperature, shear rate, and relative humidity. Near the glass transition temperature (T_g), powders exhibited an abrupt increase in static flow threshold, indicating caking due to particle agglomeration. At higher temperatures, a transition from elastic to plastic flow was observed around $80°C$, accompanied by changes in the plateau value of the shear modulus (G'_0) for different powders. In the dense flow regime, a critical temperature value dictated the transition between caking (*powder's tendency to form lumps or masses*) and free-flowing behavior, with temperature promoting agglomeration and shear rate causing dispersion. The critical temperature increased with the strain rate, highlighting the delicate balance between agglomeration and dispersion. Also, it is found that Relative Humidity (RH) plays a crucial role in reducing the stress developed within the sample and counteracting the temperature effect. Additionally, the slow compaction dynamics of powders were studied, revealing an inverse logarithmic law with a characteristic relaxation time (τ) that strongly correlated with the angle of repose.

Keywords: selective laser sintering, polyamide powders, rheology, slow compaction dynamics, agglomeration or caking, PA11, PA12.

1. Introduction

Powder materials play a pivotal role in various handling and processing tasks, impacting transportation, separation, mixing, compression, and packaging [1, 2]. Among the cutting-edge techniques for rapid prototyping, Selective Laser Sintering (SLS) stands out. It leverages an additive manufacturing (AM) process utilizing a powder bed to craft intricate polymer and composite materials, eliminating the need for traditional tooling or molding [3, 4, 5, 6, 7]. Instead, it builds layers by selectively fusing heat-fusible powdered material using a scanning laser beam. SLS excels with thermoplastic polymers like polyamide, polypropylene, and polystyrene, thanks to their low melting temperatures, with polyamide being a popular choice due to its ease of processing [8, 9].

Attaining both high process efficiency and desirable final product quality is crucial, making the optimal performance of powders a critical factor. The flow and packing characteristics of powders during layering significantly impact their performance. Inconsistent feedstock can lead to uneven bulk density, non-uniform layering, reduced tensile strength, and inferior surface finish, all of which negatively affect the final product quality [10]. The efficiency and quality of the process rely on the rheological performance of the powders, which refers to how the powder flows and packs during layer formation. The layer thickness typically ranges from 100 to 150 micrometers, limiting the maximum particle size [11]. The significance of particle size distribution is widely acknowledged in determining the thickness of each layer, thus influencing the precision of the printed component. Additionally, the shape of particles directly affects their flowability. Spherical and smooth particles exhibit easy rolling motion upon each other, while rough particles tend to make solid contact through one or a few raised areas, resulting in heightened friction between particles [12, 13, 14, 15, 16]. Consequently, in the latter case, the layer thickness lacks uniformity.

Recognizing the intricate nature of powder systems throughout all phases of the powder bed SLS process, including tasks like layer recoating and interactions between the powder and the energy source, poses a challenge. Efforts have been made to create reliable techniques for evaluating the flow behavior of powders destined for use in additive manufacturing. Within this context, "flowability" typically refers to a powder's capacity to flow, while the ability of a powder to form thin layers within an AM apparatus is often denoted as "spreadability" [17]. There isn't a universally accepted definition of flowability as a powder property; instead, various characterization methods measure distinct flow properties, collectively representing the overall flow behavior of a powder through flowability indices.

A major challenge in assessing flowability for AM is the proliferation of conflicting opinions regarding various methods, reflected in the extensive literature on the subject [18, 19, 20, 21].

*Corresponding author
Email addresses: brendan.huitorel@arkema.com (Brendan Huitorel), abdoulaye.fall@cnrs.fr (Abdoulaye Fall)

Accurately measuring or predicting the flowability of a powder remains a challenging task due to the multitude of factors influencing the flow behavior of bulk materials. Factors such as particle size distribution, particle morphology, moisture content, temperature, powder charge state, and applied stresses all come into play [22]. Consequently, various measuring devices and methods are available to assess flowability, each with distinct approaches. Notably, the stress state of the bulk material is a critical parameter, and measurement methods are categorized based on whether they evaluate the sample under an applied normal stress (e.g., ring shear tester) or without applying normal stress (methods like Hausner ratio and rotating drum) [19, 23].

To investigate the rheological behavior of polyamide powders, our focus was on two primary factors: temperature and relative humidity, known to significantly affect the flow properties of the powder. The impact of temperature on powder flowability is particularly significant, especially in processes like SLS where powder spreading occurs at elevated chamber temperatures. In the case of polyamide 12 (PA12), for example, the building chamber temperature is typically around $170°C$. It is essential to consider flowability measurements at elevated temperatures, as information solely based on ambient conditions may not accurately assess flowability during actual processing conditions. To illustrate this point, Ruggi et al. [24] employed a heated ring shear device, while Amado et al. [25] utilized a heated Revolution Powder Analyzer. Notably, both studies found that flowability declined as the temperature increased. Our aim is to gain insights into how these factors influenced the flowability of the powder and, consequently, its performance in the laser sintering process. In the context of SLS, where the polymer powder is applied with minimal axial normal stress, we have chosen to conduct rheological measurements under the imposition of normal stress. This approach allows us to investigate the flow and yielding behaviors of powders [26, 27].

2. Experimental methods

2.1. Material characterizations

For the morphological analysis, we first focused on the examination of powder particles using scanning electron microscopy (SEM) and employing image analysis techniques to extract pertinent data. Second, we involved the implementation of laser diffraction particle size analysis to obtain a particle size distribution.

The four polyamide grades, all from ARKEMA, that are selected for this study are listed in Table 1.

Polymer	Trade name	Abbreviation
Polyamide-12	Orgasol® Invent Smooth	OIS
Polyamide-12	Orgasol® 2003 LS	2003LS
Polyamide-11	Rilsan® Invent NAT	RIN
Polyamide-11	Rilsan® EXP	RXP

Table 1: Polyamide powders investigated in this study.

The morphology of polyamide powders is examined under a scanning electron microscope as shown in Fig.1 that exemplarily depicts SEM pictures of the two categories of powders studied here. The image was taken on a JEOL 6300F field emission electron microscope, at 10 kV, in high-vacuum mode. The SEM images show a difference in shape between the two powder types. Orgasol particles have a relatively regular and spherical particles with fairly uniform size of approximately $50\mu m$. Rilsan particle, on the other hand, have an irregular shape and distinct dimensions and they look fully dense structures at high magnification. Coarse and Fine particles are notably present in these powders.

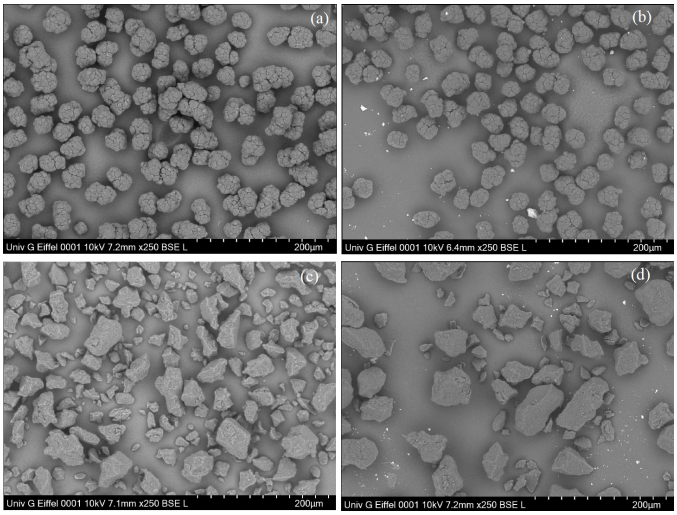

Figure 1: SEM micrograph of powders with a magnification of ×250: (*a*) O2003LS (*b*) OIS (*c*) RXP and (*d*) RIN.

It is important to note that in the OIS and RIN samples, there are visible finer particles. These fine particles are more distinct compared to the larger ones, indicating that they may consist of chemical elements with a higher atomic number. It is entirely possible that the particles with a brighter color in the image are indicative of agglomerated silica or some other contaminant. However, it is reported [28] that some powders used in the selective laser sintering process may include flowing agents such as fumed silica, which could explain the presence of these fine particles. Indeed, Dupin and coworkers [28] conducted an Energy Dispersive X-ray Spectroscopy (EDX) analysis on both the larger and finer particles to detect the potential presence of the element silicon. The analysis revealed a higher concentration of silicon and oxygen elements for the fine particles, confirming the greater presence of silica in these particles. The presence of fine silica particles serves to improve the flowability and increase the bulk density of the sintered parts. The bonding of fumed silica onto the surface of the particles helps to decrease the adhesion force between the particles.

Particle size distributions of powders were performed using a Malvern INSITEC particle size analyzer equipped with a $670nm$ laser diode and a fixed focal length of $300mm$. The data was collected using the RTSIZER software. The PSD of powders are shown in Fig. 2 and Table 2 summarizes the particle

Powder	$D_{10}(\mu m)$	$D_{50}(\mu m)$	$D_{90}(\mu m)$
OIS	26.61	36.96	57.81
O2003 LS	26.65	36.93	59.08
RIN	20.33	46.28	82.44
RXP	21.72	48.45	82.44

Table 2: PSDs of powders.

size distribution parameters for the four investigated polyamide powders.

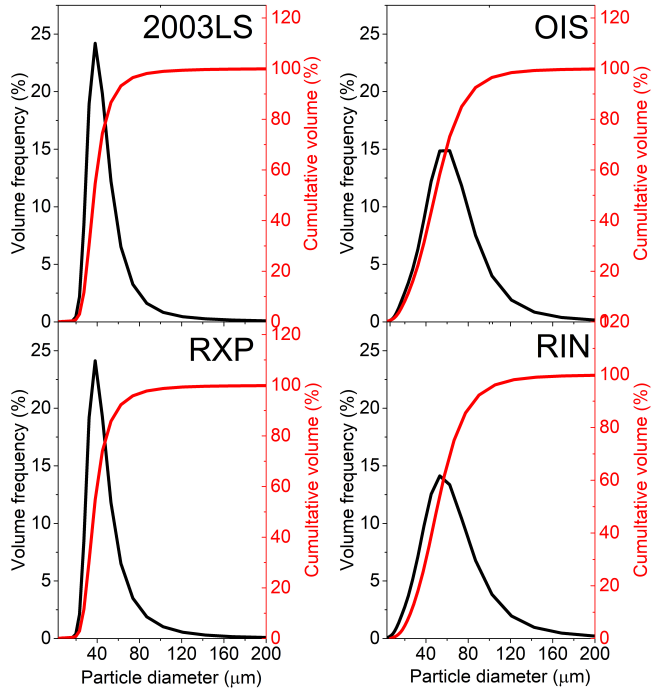

Figure 2: Linearized histograms of particle size distributions and cumulative distributions of powders.

Orgasol type powders exhibit fairly similar PSDs, covering approximately the same diameter range while RIN and RXP present a similar but wider PSD.

2.2. *Rheological measurements*

Powder materials must be confined to carry out rheometric experiments, and are conveniently characterized in shear flow under controlled normal stress [26]. Normal stress-imposed rheological measurements are carried out using a home-made plate-cup shear device (Fig. 3). The upper and the lower plate radii are $R_u = 25mm$ and $R_d = 25.05mm$. The filling height h of the plate box is adjustable from a few (typically 5) to 1000 particle diameters. To avoid wall slip, the rotating mobile upper boundary is covered with a sandpaper to which the grains may fit while the static lower cup, made of Dural is serrated and equipped with the electrically heated plate. A small amount of this powder is then introduced into the designated space. In the case of non-cohesive powders, the yield stress is relatively low, allowing the grains to reach a state resembling close packing when poured into the rheometer geometry. However, cohesive powders exhibit a higher yield stress, preventing the material from compacting under its own weight, resulting in significantly lower grain filling fractions. To enable a fair comparison among different powders and to obtain results that are not heavily influenced by the loading method, before each measurement, the sample is compacted by imposing a normal force of $10N$ which corresponds to $1666Pa$ of normal stress under $1Hz$ oscillation cycle with an angular displacement of π; allowing thus a good filling of the shear cell. In such case, the solid packing fraction reached at this initial stage is $\phi_0 = 0.62 \pm 0.005$ (for most of the experiments). This compaction process ensures reproducibility across all samples and for each loading of the compaction step. The experiments were performed using a stress-controlled rheometer (Anton Paar MCR 502), with the temperature set between 20 and $150°C$ for each sample. Measurements could not be performed above the latter due to the lack of repeatability caused by partial melting of the powder observed on the wall of the apparatus.

In a first series of experiments, a conventional strain sweep under normal force controlled, allows for the separation of the elastic and viscous properties during the yielding. The modulus, denoted as G', is subsequently evaluated at a frequency of $1Hz$. We opted for this frequency as it allows for quick measurements. We confirmed that G' remains independent of frequency within the range of 10^{-2} to $10Hz$, which encompasses the frequencies readily accessible on the rheometer. To ensure that the measurements capture the linear and elastic response, the shear strain is incrementally increased throughout a single experiment during a $22.5min$ logarithmic ramp from 10^{-6} to 10^{-3}. Dynamic storage G' and loss G'' moduli are hence measured as a function of the strain amplitude. For a given temperature and/or relative humidity, a minimum of three such measurements are conducted for each powder.

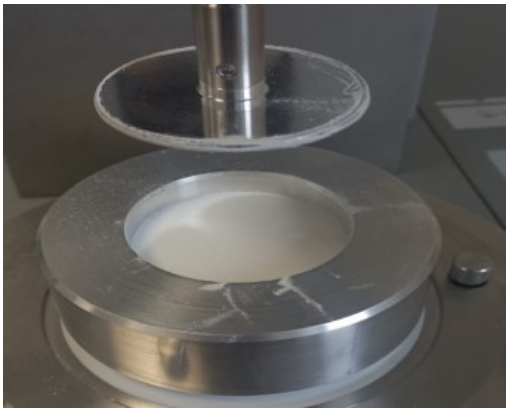

Figure 3: Plate-cup shear device.

In a second set of experiments, we utilize a vane-in-cup geometry to investigate the flow behavior of the powders. As the formation of caking in these powders is influenced by temperature, their rheological properties also exhibit temperature dependence. By subjecting the powder to a sufficiently high shear

rate, the system undergoes homogenization. However, at low shear rates, the presence of caking induces a yield stress, causing the viscosity to increase exponentially with temperature, eventually reaching an infinitely high viscosity in a steady state. The vane-in-cup geometry used for the experiments consists of six vanes of 16*mm* in height and a inner radius of 11*mm* and a cup outer radius of 22*mm*. The cup, made of Dural is serrated in order to avoid wall slip.

3. Results and Discussion

Figure 4 shows a generic behavior of storage modulus G' as a function of the strain amplitude γ for different temperature. For small strain amplitude, G' is independent of the applied strain amplitude and G' is always larger than the loss modulus G'' (not shown for clarity), which corresponds to a linear viscoelastic behavior and elastic domination. Then, the dynamic moduli decrease with a constant slope. Moreover, it is interesting to see that the plateau value G'_0 of the shear modulus, depending of the powder type, is strongly affected by the temperature: it increases with increasing the applied temperature for Orgasol type powders (PA12) while it stays roughly constant in RIN and RXP powders (PA11).

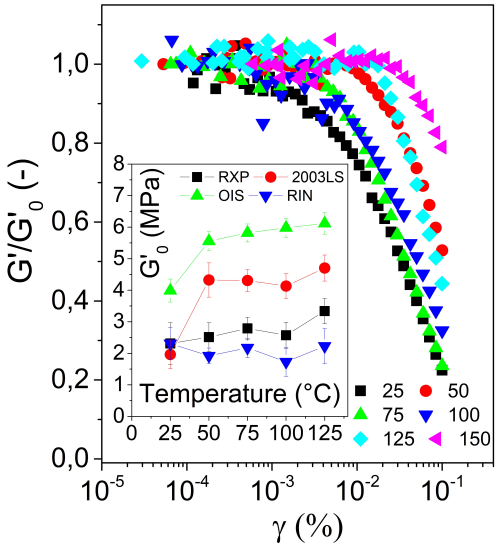

Figure 4: Dimensional generic shear modulus G'/G'_0 as a function of strain for several set temperature for the RIN powder. The inset shows how G'_0 evolves with temperature within the powder types.

It is well known that polyamide powders can undergo thermal softening above the glass transition temperature T_g which generally falls within a range of approximately $40°C$ to $70°C$, leading to increased stickiness and caking tendencies [29]. Caking phenomenon refers to the undesirable agglomeration behavior of powders, resulting in the formation of solid lumps or clusters. When powders are exposed to moisture, temperature changes, or prolonged storage, the fine particles may stick together, forming larger aggregates. In this study, we measured the glass transition and melting temperatures of the four powders using Differential Scanning Calorimetry (DSC). The instrument employed was a TA Q2000 DSC with an intracooler for cooling purposes. The ramp rate was set at 20°C/min for each thermogram. The obtained values are summarized in the following table 3:

Powders	OIS	O2003LS	RIN	RXP
$T_g(°C)$	45.9	41.9	50.2	52.5
$T_f(°C)$	181.4	182.1	201.5	186.4

Table 3: Glass transition and melting temperatures of the four powders.

Caking in powders can result from various mechanisms, including interparticle forces like van der Waals forces or capillary forces, as well as the presence of moisture acting as a binding agent. In our case, temperature changes appear to be the primary cause of caking. This suggests that temperature variations play a more dominant role in inducing particle agglomeration and caking compared to moisture content in the given experimental conditions. Furthermore, the results depicted in Figure 4 indicate that increasing the temperature expands the linear regime, indicating that the yielding behavior of the powder becomes more pronounced with temperature. This yielding behavior can be attributed primarily to the frictional or adhesive properties of the particles in contact under the applied temperature [30].

The rheology of powders is primarily governed by momentum transfer and energy dissipation that occur through direct contacts between particles as well as with the surrounding walls. At low strain rates, particles remain in contact and interact frictionally with their neighboring particles over extended periods of time. As the deformation rate increases, a transition to a viscous-like regime occurs, and the powder starts to flow more like a liquid [31]. In this intermediate regime, particles experience multiple contact interactions. At very high strain rates, a transition takes place towards a gaseous regime, where particle interactions primarily occur through binary collisions [32].

The interactions between particles, which govern powder flowability, can exhibit complex and pronounced dependencies on temperature. Studies on various materials such as lactose, coffee, waxes, and fly ashes have demonstrated this effect [33, 34, 35]. For example, adhesion forces can increase with rising temperature due to changes in adsorption layers, liquid bridges, and contact areas due to visco-plastic deformation. Alternatively, flowability can decrease due to the formation of solid bridges during sintering [36, 37]. These temperature-induced changes in particle interactions can have a substantial impact on the overall flow behavior of powders, and therefore, it is crucial to study flowability at the relevant processing temperatures.

To investigate this behavior further, in the second set of experiments, we conducted measurements to determine the steady-state behavior in the quasistatic as well in the dense flow regimes. For this purpose, we applied different temperature values and monitored the resulting shear stress over time at a constant shear rate.

In the quasistatic regime, specifically when the applied strain rate is very low, several distinct stages of behavior are observed

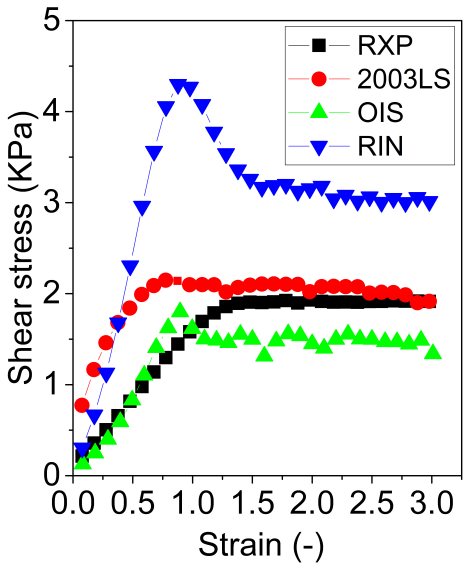

Figure 5: Steady shear stress versus strain when slowly shearing powders from rest at $0.01s^{-1}$.

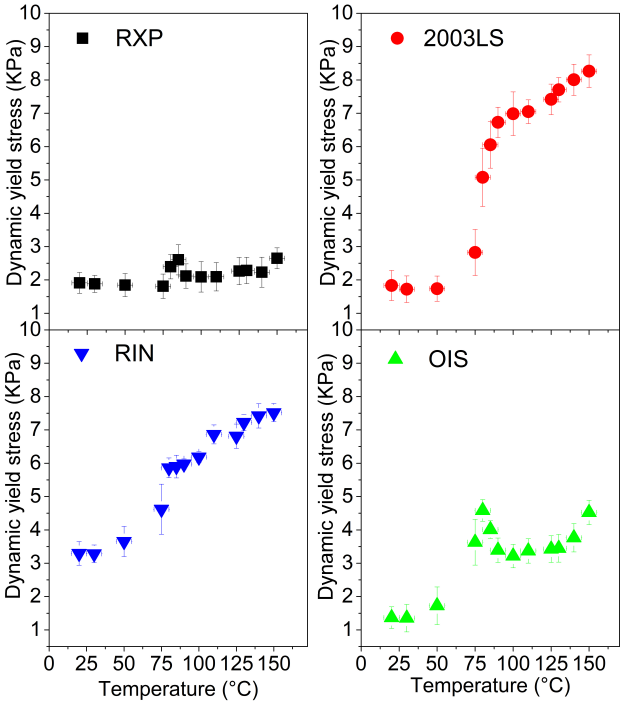

Figure 6: Dynamic yield stress versus Temperature when slowly shearing powders from rest at $0.01s^{-1}$.

as shown in Figure 5. Initially, at room temperature, namely $20 - 30°C$, we have a generic behavior : the stress-strain relation exhibits a simple expected linear behavior ($\sigma \simeq 2G'_0\gamma$) similar to that of an elastic solid. This indicates that the powder has a yield stress, and at this stage, stress levels are quite high. Following the initial linear increase in stress, there is an overshoot at strain of about unity and a short plateau phase, which corresponds to a plastic flow regime. During this phase, the material undergoes plastic deformation, implying that it experiences permanent changes in shape and retains some degree of fluid-like behavior. This plateau may define the **dynamic yield stress** σ_y of the powder materials whereas the maximum stress before the overshoot represents the static yield stress. Noticed that the non-cohesive powder RIN exhibits the highest static flow threshold and this observation is in total line with its particle size distribution shown in Fig.1 and Fig.2. Indeed, this powder has a highly polydisperse particle size distribution, with angular grains. This combination of granulometric features can contribute to an elevated static flow threshold for the powder.

In Figure 6, we plot the plateau value $-\sigma_y-$ as the function of temperature. At $50°C$, σ_y starts to increase, then remains linear with temperature until $80°C$. This sharp increase in shear stress threshold $-\sigma_y-$ is observed in almost all powders studied, except in the case of RXP, where the increase is moderate. The occurrence of this sharp increase at around $50°C$ suggests that a significant change in the mechanical properties of the powder materials is happening at this temperature range. This behavior is likely associated with the proximity to the glass transition temperature (T_g) of the powder. Since, polyamide powders are semi-crystalline materials, they possess a glass transition temperature [38]. Below T_g, polyamide powders exhibit a rigid, glassy behavior. The polymer chains are typically frozen in place, and the particles maintain a relatively fixed position in the material. Interparticle cohesive forces in this state are generally driven by intermolecular forces such as van der Waals forces and hydrogen bonding. These forces may not be as dynamic, given the restricted movement of polymer chains.

As the temperature approaches T_g, the polymer chains start to gain mobility, and the material transitions from a glassy to a rubbery state [39, 40, 41, 42]. In this transition region, there could be an increase in intermolecular interactions. The chains become more mobile, allowing for greater contact and potential entanglement between particles, leading to enhanced interparticle cohesive forces. Above T_g, polyamide powders enter a rubbery state, resembling a liquid-like behavior. The polymer chains have significant freedom of movement. The increased mobility of polymer chains allows for more extensive intermolecular interactions. This enhanced cohesion can result in better particle-particle adhesion, potentially leading to the formation of agglomerates or larger clusters as it can be seeing in Figure 7.

Figure 7: Pictures of caked powders

As the temperature is further increased, the polymer chains

have high mobility, leading to enhanced interparticle cohesion and adhesion. The material becomes flexible, deformable, and shows reduced friction. For instance, in the case of RIN powder, above $80°C$, the shear modulus decreases dramatically from $55768 \pm 5000Pa$ to $5715 \pm 500Pa$, indicating a considerable decrease in the resistance to shear deformation. And far above the glass transition temperature but below the temperature of fusion, semi-crystalline polyamide powders exhibit elastomeric behavior, the stress-strain relationship remains linear, but the slope of the curve becomes smaller, indicating a decrease in the shear modulus which falls to $989 \pm 90Pa$.

However, above $80°C$, the behavior of OIS and RXP is different from what was observed before. For these two powders, an overshoot phenomenon is observed just after this temperature. The shear stress decreases and saturates with deformation, indicating a transition from an elastic regime to a plastic regime at a critical temperature of $80°C$. This overshoot behavior is indicative of a sudden reduction in the resistance to shear deformation, leading to a decrease in shear stress. It suggests that these powders undergo a change in their mechanical response, becoming more deformable and flowable at temperatures above $80°C$. The transition from an elastic regime to a plastic regime implies that the powders start to exhibit more fluid-like behavior with increasing temperature. The critical temperature of $80°C$ appears to be significant for both OIS and RXP, as it marks the point where their flow behavior undergoes a fundamental change. This behavior may be attributed to changes in particle-particle interactions, adhesive forces, or other physical properties that come into play at this temperature and could be a consequence of the material reaching or surpassing its glass transition temperature, leading to a softer and more flowable state.

We turn now to the dense flow regime. In this regime however, a generic behavior is observed whatever the powder is and for clarity, we are focusing on RIN powder. The steady stress measurements, shown in Figure 8a, revealed the presence of a critical temperature value, around which the steady stress increased. When the temperature was slightly below the critical value, the stress exhibited a continuous decrease towards lower values, indicating a tendency for the system to flow freely. For temperatures slightly above the critical value, we observed that the stress increased continuously with temperature. This behavior indicates that the system undergoes caking, demonstrating the ability of the particles to agglomerate with temperature even in the dense flow regime.

More quantitatively, repeating this experiment for different strain rates, one can obtain the critical temperature change as a function of the strain rate that allows the powder to flow freely, i.e., without developing caking due to particle agglomeration (Figure 8b).

Thereby, we observe a competition between temperature and strain rate in this system. The effect of temperature is to promote particle agglomeration, leading to the formation of larger clusters or caking. On the other hand, shear has a dispersing effect, causing the particles to separate and redistribute. These opposing influences result in a delicate balance between agglomeration and dispersion, which is manifested by the observed changes in stress and flow behavior. Increasing the strain rate leads to an increase in the critical temperature, allowing the system to flow, until the agglomeration disappears altogether: the stress is back to low values. This unambiguously demonstrates that the caking is an agglomeration effect, and that taking away a particle contact factor makes the caking disappear altogether.

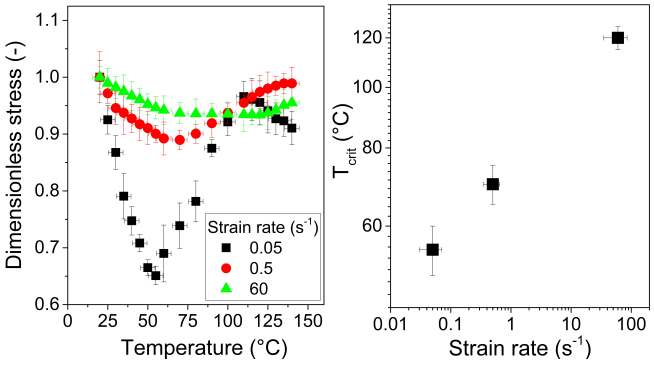

Figure 8: a) Dimensionless Shear stress versus temperature when shearing RIN powder from rest at different strain rates. b) Critical temperature T_{crit} versus strain rate.

To further investigate the powder behavior and its response to different environmental conditions, we vary the relative humidity. By altering the relative humidity, we can explore how changes in moisture content affect the powder's flowability and agglomeration tendencies. The humidity level is controlled by exposing the samples to a well-known humidity atmosphere. The samples are placed inside desiccators under constant humidity conditions. The humidity is controlled using a solution of salt dissolved in distilled water present in the lower part of the enclosure, as shown in the figures below. The prepared solutions provide two controlled atmospheres with humidity levels of 53.5% (Magnesium Nitrate Hexahydrate solution) and 97% (Potassium Sulfate solution).

To ensure accurate measurements, the relative humidity is constantly monitored using a hygrometer. The hydrophilicity of polyamides is influenced by several factors, including the presence of polar groups and the length of the carbon chain within the polymer. PA6 (Polyamide 6) is known for its relatively high water absorption capacity compared to some other polyamides. Its ability to absorb water, ranging from 3-10% of its weight, is attributed to the polar amide groups and the structure of the polymer chain. PA12, on the other hand, is generally less hydrophilic than PA6. It can absorb a lower percentage of water, approximately 0.2-1% of its weight [43]. This is likely due to differences in its molecular structure, which affects its interaction with water molecules. For this reason, samples are left inside the enclosures for an extended period of around two weeks, maximizing their exposure to the humidified air. This controlled exposure allows for the study of the powders' behavior under different humidity conditions, providing valuable insights into the effects of moisture on their flow and mechanical properties.

Both the dry and moist samples exhibit a generic behavior

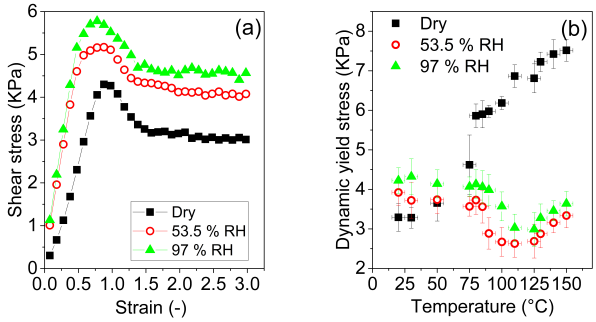

Figure 9: a) Shear stress-strain curves for slowly shearing RIN powders from rest at a shear rate of $0.01s^{-1}$ at $20°C$ for three RH values. b) Dynamic yield stress versus Temperature for three RH values.

at room temperature ($20 - 30°C$). The stress-strain relation initially shows a linear rise, indicating the presence of a yield stress, and then enters a plastic flow regime with a short plateau phase, indicating plastic deformation and fluid-like behavior. However, stress levels are higher in the moist samples compared to the dry ones at this stage [27, 44].

Below $75°C$, σ_y stays constant, indicating an effect that delays caking. This observation is consistent with established knowledge regarding powder behavior. Notably, there is empirical support for the efficacy of maintaining storage conditions below 33% relative humidity in averting severe caking in dairy powders, as elucidated by Listiohadi et al. [45, 46, 47]. However, above $75°C$, the behavior changes for the moist samples: the dynamic yield stress decreases with temperature before to increase when temperatures reach $110°C$. This suggests a more pronounced yielding due to caking in the dry powder. It is worthwhile to note that the drying dynamics, particularly at elevated temperatures, could significantly contribute to the observed variations in the sense that above $110°C$, the difference in σ_y, as observed here, may be attributed to the residual sample humidity.

Additionally, the density of the powder bed before the laser passes through significantly influences the final properties of the sintered parts. Consequently, it becomes crucial to characterize the bulk and tapped density of powders and understand their behavior during flow.

The packing fraction measures the efficiency of how tightly particles in a powder material can be packed together. It represents the ratio of the volume occupied by the particles to the total volume available. A higher packing fraction indicates that the particles are densely packed and occupy a smaller volume with fewer voids. Conversely, when the packing fraction is small, approaching zero, it indicates that the material has poor packing behavior. This means that there are many empty spaces or voids within the unit volume, and the particles are not efficiently filling the available space. A low packing fraction suggests that the particles are not closely packed together, leading to a lower density and potentially reduced material properties such as flowability or mechanical strength.

Before the vibration, the container, made of PMMA, were first cleaned using distilled water and then dried in an oven at 60°C. Subsequently, each powder with a mass of $300g$ is gently poured into the container –of volume V_c– which is fixed on the *Octagon 200 sieve shaker* to form an initial packing. Then, the container with the initial binary packing is vibrated under a pre-determined vibrational condition (vertical shaking with an amplitude 5) for a period of time and the packing density is measured as:

$$\phi = \frac{V_p}{V_c} = \frac{m_p}{\rho_p} \times \frac{4}{\pi D^2 \bar{H}} \tag{1}$$

where m_p and $\rho_p \simeq 1.05 g/cm^3$ represent the mass and theoretical density of particles, $\bar{H}$ represents the mean height of the packing structure, and D is the inner diameter of the container.

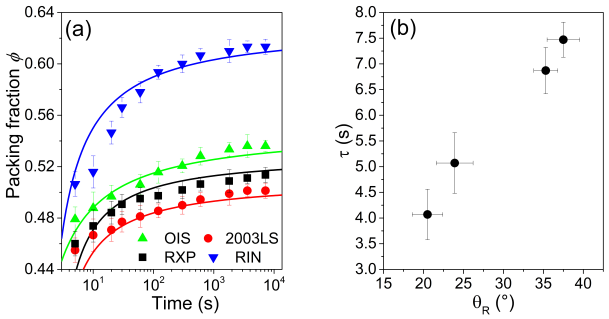

Figure 10: a) Time evolution of the mean packing fraction ϕ of powders. Solid lines are the fits using the inverse logarithm law (2). The free fitting parameters are k, ϕ_c, and τ, respectively, while ϕ_0 is measured at the beginning of the experiment. b) Experimental data of the relaxation time τ as a function of the angle of repose θ_R of powders.

The compaction curves, represented by $\phi(t)$, for powders are illustrated in Figure 10a using a semilog plot. Remarkably, the rough Rilsan powder (RIN) displays a significantly higher packing density in comparison to the other powders. As previously mentioned, this powder exhibits exceptional flowability, which could potentially be attributed to the inclusion of additives like silica that reduce inter-particle friction. The combination of improved flowability and a considerable proportion of smaller particles in this powder contributes to the enhanced packing efficiency observed for the specified layer thickness.

Furthermore, these packing curves show a similar trend characterized by slow compaction dynamics: initially increasing to a high value with time t and then reaching a constant level. Previous studies, such as those by Knight et al. [48] and Fiscina et al. [49], have reported that dry granular assemblies follow an inverse logarithmic law described by the equation:

$$\frac{\phi(t) - \phi_0}{\phi_c - \phi_0} = 1 - \frac{1}{1 + k \log\left(\frac{t}{\tau}\right)} \tag{2}$$

In this equation, $\phi(t)$ represents the packing density at time t, ϕ_0 is the initial packing density, ϕ_c is the maximum achievable packing density, k is a constant parameter, and τ represents a characteristic time scale. The relaxation time τ plays a crucial role in understanding the physics of dense random packings. It

represents a characteristic time scale associated with the compaction process.

Powders	θ_R [°]	$\phi_0[-]$	$\phi_c[-]$	$k[-]$	$\tau[s]$	Nature
OIS	23.9	0.47	0.55	0.43	5.07	Non cohesive
2003 LS	35.3	0.44	0.51	0.63	6.87	Cohesive
RIN	20.5	0.50	0.63	0.7	4.07	Non cohesive
RXP	37.5	0.46	0.53	0.63	7.47	Cohesive

Table 4: Nature of powders investigated in this study and the fit parameters from Eq. 2

So, we have measured the stability of a pile of powders and as expected, the relaxation time is seen (Figure 10b) to increase dramatically with the angle of repose θ_R confirming the idea that particle interactions play an important role in the cohesive powders. Indeed, the repose angle, also known as the angle of repose, is a characteristic property of granular materials. It refers to the maximum stable angle at which a pile of granular material can be formed without collapsing or flowing [19]. Technically, a cone is formed by dropping the material through a funnel of standardized dimensions (according to ISO 6186) and the angle considered is the inner one formed between the slant height and the horizontal plane. The smaller the angle of repose is, the higher the flowability is. This strong effect means that for large θ_R values, which occurs in cohesive powders (see Table 4), rearrangements involving the motion of grains become rare events. The relationship between the relaxation time and the repose angle can be understood in terms of the stability of the granular assembly. A longer relaxation time allows for more internal rearrangements and the formation of a more stable packing structure, leading to a higher repose angle. Conversely, a shorter relaxation time limits the ability of the particles to reorganize, resulting in a lower repose angle. This confirms the cohesive effect of powders over compaction experiments.

Indeed, Boutreux and de Gennes developed a free volume model that supports the inverse logarithmic dynamics observed in compaction processes [50]. This model considers the relationship between compaction and grain mobility. In their study, they found that this relationship can be described by the Vogel-Fulcher-Tammann law that is a phenomenological equation frequently used to describe the temperature dependence of relaxation times in glass-forming materials. Also, the work of Philippe and Bideau [51] suggests a relationship between such relaxation time τ and the tapping intensity Γ, which represents the maximal acceleration experienced by the packing during tapping. According to their findings, the relaxation time can be approximated by an exponential function of the form $\tau \approx \exp(\Gamma_0/\Gamma)$. Here, Γ_0 represents a parameter related to the existence of an energy barrier that needs to be overcome for the particles in the packing to undergo relaxation. The presence of this energy barrier indicates that there are certain constraints or interactions within the packing that affect the relaxation process. As the tapping intensity increases, the energy barrier is gradually overcome, allowing the particles to rearrange and leading to a decrease in the relaxation time.

4. Conclusion

In conclusion, this comprehensive study on the rheological behavior of semi-crystalline Polyamide powders for Selective Laser Sintering provides valuable insights into their complex dynamics under different environmental conditions. Our results highlight the impact of temperature, shear rate, and relative humidity on powder flow properties and demonstrates how these factors contribute to phenomena like caking and plastic flow. The results reveal critical temperature values that influence the transition between caking and free-flowing behavior, with relative humidity playing a crucial role in reducing stress and opposing the temperature effect. The findings also unveil the slow compaction dynamics of powders, showing a correlation between relaxation time and the angle of repose.

This work contributes to a better understanding of powder handling and processing, particularly in selective laser sintering and other industrial applications. The knowledge gained from this study can be instrumental in optimizing manufacturing processes and product quality, ultimately benefiting various industries that rely on powder materials. Further research in this field promises to unlock even more profound insights, leading to advancements in powder science and engineering.

Acknowledgements

We extend our appreciation to David Hautemayou and Cédric Mézière for their technical support. Special thanks to P. Belin for providing SEM images, which have greatly contributed to our work. Additionally, A. Fall expresses gratitude to Anton Paar France for lending the powder cell, which we utilized to validate our findings obtained with the homemade shear cell. B. Huitorel thanks the R&D teams of CERDATO Research Center.

Author contribution statement

MM and AF carried out the experiments, implementing methods supplied by AF; AF prepared the figures in their final form and wrotes the paper, which was thoroughly reviewed by MM and BH.

References

[1] R. Freeman, Powder Technology **174**, 25 (2007).
[2] J. Duran, *Sands, powders, and grains: an introduction to the physics of granular materials* (Springer Science & Business Media, 2012).
[3] G. Salmoria, J. Leite, C. Ahrens, A. Lago, and A. Pires, Polymer Testing **26**, 361 (2007).
[4] P. K. Jain, P. M. Pandey, and P. Rao, The International Journal of Advanced Manufacturing Technology **43**, 117 (2009).
[5] A. Amado-Becker, J. Ramos-Grez, M. J. Yañez, Y. Vargas, and L. Gaete, Rapid Prototyping Journal **14**, 260 (2008).
[6] H. Zarringhalam, N. Hopkinson, N. Kamperman, and J. De Vlieger, Materials Science and Engineering: A **435**, 172 (2006).
[7] L. Lü, J. Fuh, and Y.-S. Wong, *Laser-induced materials and processes for rapid prototyping* (Springer Science & Business Media, 2001).
[8] J.-P. Kruth, X. Wang, T. Laoui, and L. Froyen, Assembly Automation (2003).
[9] R. Goodridge, C. Tuck, and R. Hague, Progress in Materials science **57**, 229 (2012).

[10] A. E. Tontowi and T. Childs, Rapid Prototyping Journal **7**, 180 (2001).
[11] L. Verbelen, S. Dadbakhsh, M. Van den Eynde, J.-P. Kruth, B. Goderis, and P. Van Puyvelde, European Polymer Journal **75**, 163 (2016).
[12] K. Yamane, T. Tanaka, Y. Tsuji, M. Nakagawa, and S. A. Altobelli, in *Proceedings of the 1995 ASME/JSME Fluids Engineering and Laser Anemometry Conference and Exhibition* (1995).
[13] T. Oshima, Y.-L. Zhang, M. Hirota, M. Suzuki, and T. Nakagawa, Advanced Powder Technology **6**, 35 (1995).
[14] E. Lahdenpää, M. Niskanen, and J. Yliruusi, European journal of pharmaceutics and biopharmaceutics **42**, 177 (1996).
[15] R. Zou and A.-B. Yu, Powder technology **88**, 71 (1996).
[16] L. C. Chan and N. W. Page, Powder Technology **90**, 259 (1997).
[17] Y. Zhang, L. Wu, X. Guo, S. Kane, Y. Deng, Y.-G. Jung, J.-H. Lee, and J. Zhang, Journal of Materials Engineering and Performance **27**, 1 (2018).
[18] I. Baesso, D. Karl, A. Spitzer, A. Gurlo, J. Günster, and A. Zocca, Additive manufacturing **47**, 102250 (2021).
[19] D. Geldart, E. Abdullah, A. Hassanpour, L. Nwoke, and I. Wouters, China Particuology **4**, 104 (2006).
[20] D. Schulze, *Powders and bulk solids* (Springer, 2021).
[21] J. Schwedes, Granular matter **5**, 1 (2003).
[22] D. Ruggi, M. Lupo, D. Sofia, C. Barrès, D. Barletta, and M. Poletto, Powder technology **370**, 288 (2020).
[23] M. Rüther, S. H. Klippstein, S. Ponusamy, T. Rüther, and H.-J. Schmid, Powder Technology **422**, 118460 (2023).
[24] D. Ruggi, C. Barrès, J.-Y. Charmeau, R. Fulchiron, D. Barletta, and M. Poletto, Additive Manufacturing **33**, 101143 (2020).
[25] A. Amado, M. Schmid, and K. Wegener, *Flowability of SLS powders at elevated temperature*, Tech. Rep. (ETH Zurich, 2014).
[26] A. Fall, G. Ovarlez, D. Hautemayou, C. Mézière, J.-N. Roux, and F. Chevoir, Journal of rheology **59**, 1065 (2015).
[27] A. Awdi, C. Chateau, F. Chevoir, J.-N. Roux, and A. Fall, Journal of Rheology **67**, 365 (2023).
[28] S. Dupin, O. Lame, C. Barrès, and J.-Y. Charmeau, European Polymer Journal **48**, 1611 (2012).
[29] D. T. Pham, K. Dotchev, and W. Yusoff, Proceedings of the Institution of Mechanical Engineers, Part C: Journal of Mechanical Engineering Science **222**, 2163 (2008).
[30] R. Chirone, D. Barletta, P. Lettieri, and M. Poletto, Powder Technology **288**, 379 (2016).
[31] Y. Forterre and O. Pouliquen, Annu. Rev. Fluid Mech. **40**, 1 (2008).
[32] J. T. Jenkins and S. B. Savage, Journal of fluid mechanics **130**, 187 (1983).
[33] M. Ripp and S. Ripperger, Chemical Engineering Science **65**, 4007 (2010).
[34] H. Kamiya, A. Kimura, T. Yokoyama, M. Naito, and G. Jimbo, Powder Technology **127**, 239 (2002).
[35] B. Zimmerlin, H. Leibold, and H. Seifert, Powder technology **180**, 17 (2008).
[36] C. Kanaoka, M. Hata, and H. Makino, Powder Technology **118**, 107 (2001).
[37] I. Tomasetta, D. Barletta, and M. Poletto, Advanced Powder Technology **24**, 609 (2013).
[38] B. Bhandari and T. Howes, Journal of food engineering **40**, 71 (1999).
[39] Y. Roos, Journal of food engineering **24**, 339 (1995).
[40] Y. H. Roos and S. Drusch, *Phase transitions in foods* (Academic Press, 2015).
[41] D. Tabor, *Gases, liquids and solids: and other states of matter* (Cambridge university press, 1991).
[42] J. P. Cruz-Tirado, J. P. Martins, B. D. F. Olmos, R. Condotta, and L. E. Kurozawa, Powder Technology **386**, 20 (2021).
[43] L. Razumovskii, V. Markin, and G. Y. Zaikov, Polymer Science USSR **27**, 751 (1985).
[44] S. Deboeuf and A. Fall, Journal of Rheology **67**, 909 (2023).
[45] Y. D. Listiohadi, J. Hourigan, R. W. Sleigh, and R. J. Steele, Australian journal of dairy technology **60**, 214 (2005).
[46] Y. D. Listiohadi, J. Hourigan, R. W. Sleigh, and R. J. Steele, Australian journal of dairy technology **60**, 207 (2005).
[47] Y. D. Listiohadi, J. Hourigan, R. W. Sleigh, and R. J. Steele, Australian journal of dairy technology **60**, 19 (2005).
[48] J. B. Knight, C. G. Fandrich, C. N. Lau, H. M. Jaeger, and S. R. Nagel, Physical review E **51**, 3957 (1995).
[49] J. Fiscina, G. Lumay, F. Ludewig, and N. Vandewalle, Physical review letters **105**, 048001 (2010).
[50] T. Boutreux and P. de Gennes, Physica A: Statistical Mechanics and its Applications **244**, 59 (1997).
[51] P. Philippe and D. Bideau, Europhysics Letters **60**, 677 (2002).